SAFRAN SA

A model of ultrasonic reflection matrix for multiple scattering evaluation in the context of non-destructive testing

Cécile Brütt
Alexandre Aubry
Benoît Gérardin
Arnaud Derode
Claire Prada

SAFRAN

Institut Langevin
ONDES ET IMAGES

Use of titanium alloys for aeronautics

Titanium alloys advantages:

- light materials
- highly resistant to corrosion
- high mechanical properties

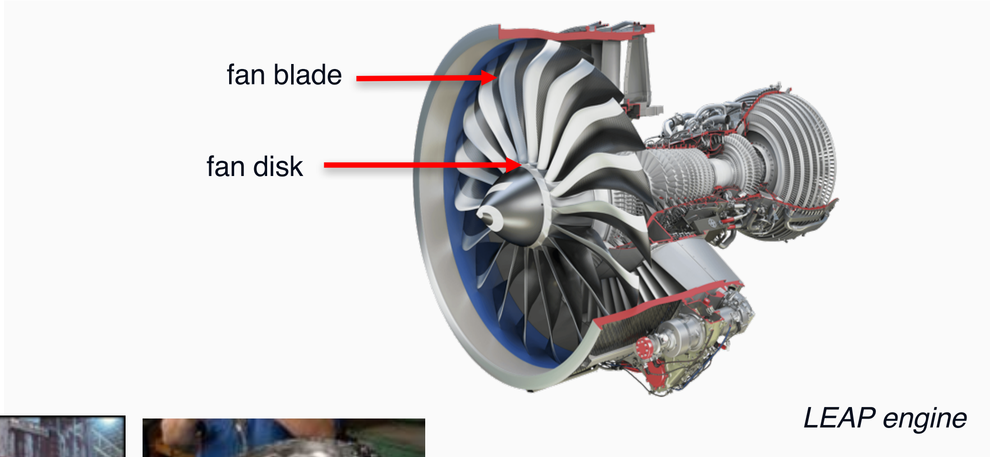

LEAP engine

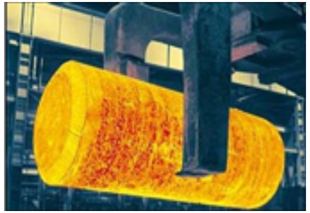
Ingot


Billet


Forged part


Finished part

Lütjering, G. & Williams, J. C. *Titanium*. (2007). Combres, Y. *Propriétés du titane et de ses alliages*. (1999).

Studied titanium alloys

Half-billets made of TA6V and Ti17

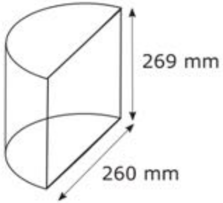

Grain flow and cristallographic texture visualisation

TA6V: elongated grains

Ti17: equiaxed grains

Micrography

EBSD

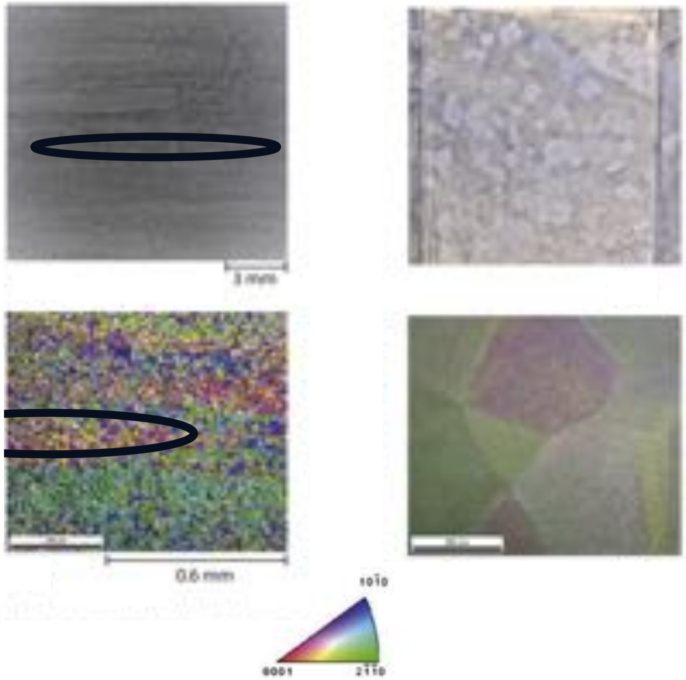

A. Baelde et al., Ultrasonics **82**, 379 (2018).

Flaws in titanium alloys parts

Sioux City crash landing (1989)
failure of the fan disk during the flight

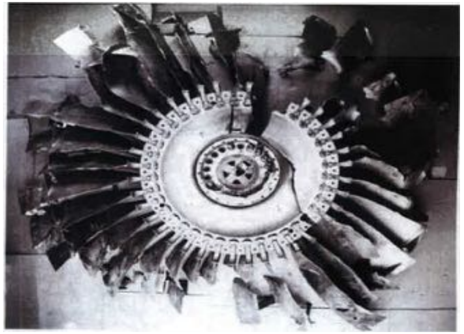

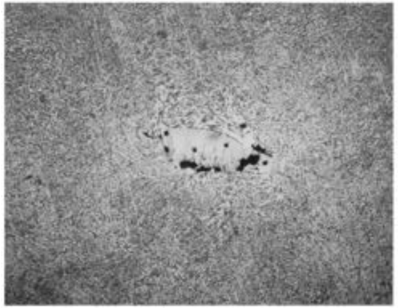

hard-α 200 µm

AIRBUS A380-861
emergency landing (2017)
crack in a hub blade slot

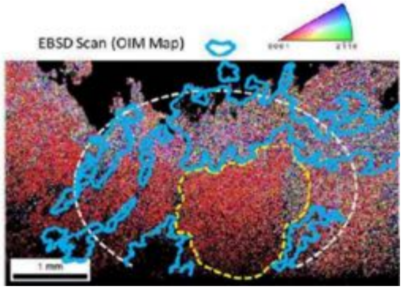

macrozone (MTR)

NTSB, *United Airlines Flight 232*. BEA, *Investigation report - Accident to the AIRBUS A380-861*.

Ultrasonic imaging

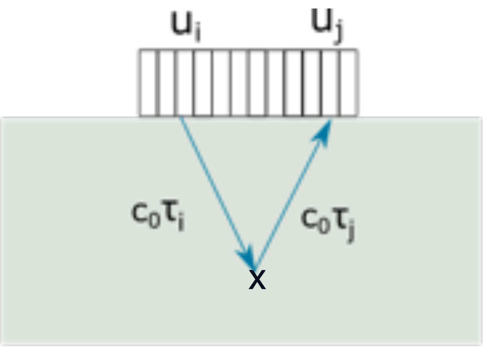

Two hypotheses to image a medium:

- the wave speed in the material is constant and known, noted c_0 ;
- received signals come from single scattering only.

Canonical basis

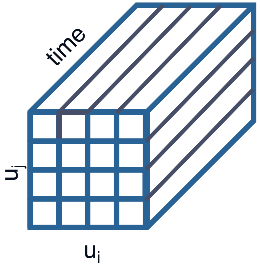

$K_{ij}(t)$

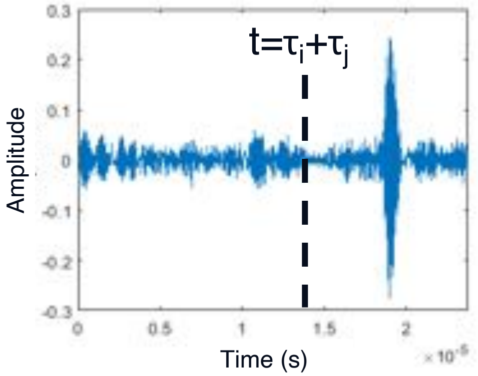

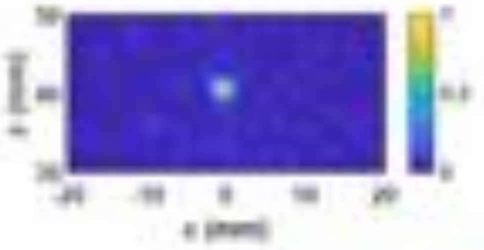

2 mm flaw imaged at 2.5 MHz

A. Velichko, IEEE Trans. Ultrason., Ferroelect., Freq. Contr. **67**, 92 (2020).

Multiple scattering contribution

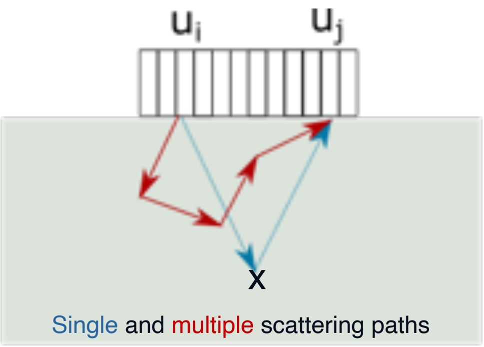

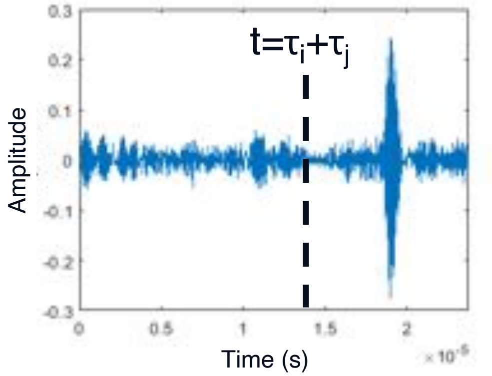

Two hypotheses to image a medium:

- the wave speed in the material is constant and known, noted c_0 ;
- received signals come from single scattering only.

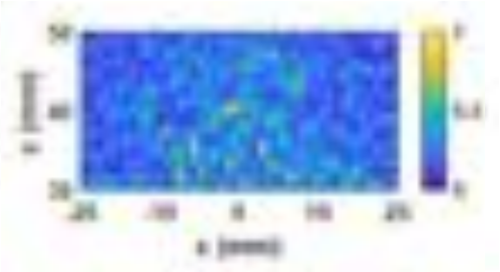

2 mm flaw imaged at 4.7 MHz

A. Velichko, IEEE Trans. Ultrason., Ferroelect., Freq. Contr. **67**, 92 (2020).

Memory effect in the single scattering regime

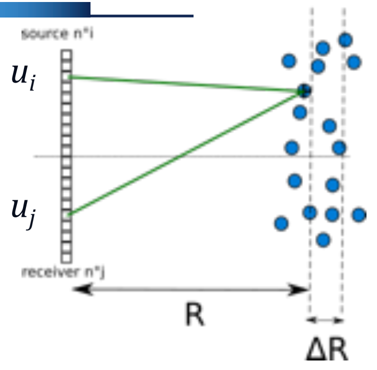

N_d scatterers with random positions X_d around depth R :

$$K(R,i,j) \propto \underbrace{\exp\left(\frac{jk(u_i - u_j)^2}{4R}\right)}_{\text{deterministic}} \underbrace{\sum_{d=1}^{N_d} T_d \exp\left(\frac{jk(u_i + u_j - 2X_d)^2}{4R}\right)}_{\text{constant along an anti-diagonal}}$$

Hypotheses :

- simple scattering
- paraxial approximation

T_d : scattering amplitude

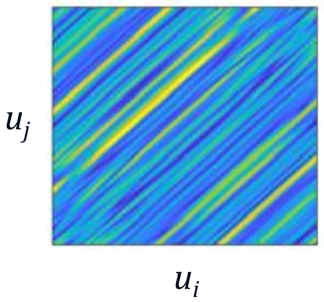

« memory effect » in the single scattering regime

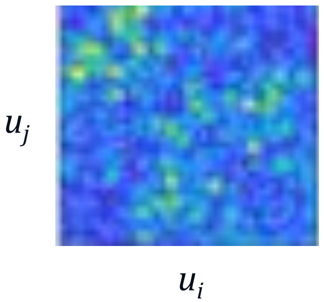

loss of the memory effect in the diffusive regime

A. Aubry and A. Derode, Phys. Rev. Lett. **102**, 084301 (2009)   A. Baelde et al., Ultrasonics **82**, 379 (2018).

Theoretical single scattering space

$$K(R,i,j) \propto \underbrace{\exp\left(\frac{jk(u_i-u_j)^2}{4R}\right)}_{\text{phase law along an anti-diagonal}} \sum_{d=1}^{N_d} T_d \exp\left(\frac{jk(u_i+u_j-2X_d)^2}{4R}\right)$$

$$E_m(R,i,j) = \begin{cases} 0 \text{ si } i+j \neq m+1 \\ \dfrac{\exp\left(\frac{jk(u_i-u_j)^2}{4R}\right)}{\sqrt{\min(m,2N-m)}} & \text{else} \end{cases}$$

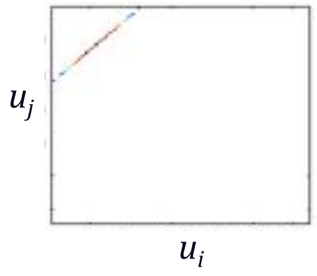

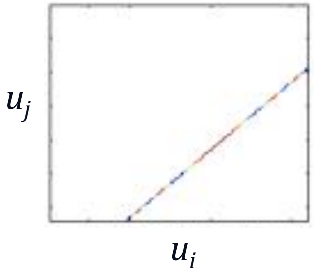

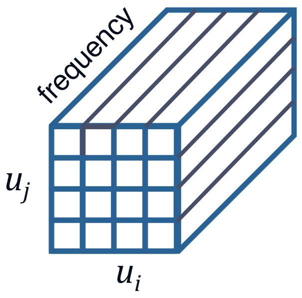

reflection matrix: **K**

Projection onto the single scattering basis

$$\boldsymbol{K_f} = \sum_{m=1}^{2N-1} \langle \boldsymbol{K} | \boldsymbol{E_m} \rangle \boldsymbol{E_m}$$

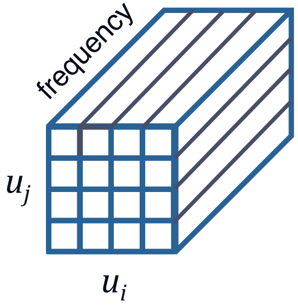

filtered matrix: $\mathbf{K_f}$

A. Baelde et al., Ultrasonics **82**, 379 (2018).

Theoretical single scattering space

$$K(R,i,j) \propto \underbrace{\exp\left(\frac{jk(u_i-u_j)^2}{4R}\right)}_{\text{phase law along an anti-diagonal}} \sum_{d=1}^{N_d} T_d \exp\left(\frac{jk(u_i+u_j-2X_d)^2}{4R}\right)$$

$$E_m(R,i,j) = \begin{cases} 0 \text{ si } i+j \neq m+1 \\ \dfrac{\exp\left(\frac{jk(u_i-u_j)^2}{4R}\right)}{\sqrt{\min(m,2N-m)}} & \text{else} \end{cases}$$

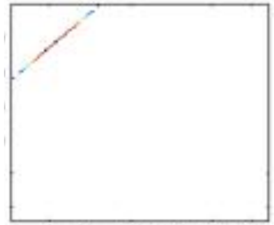

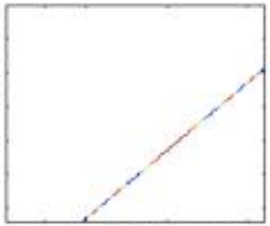

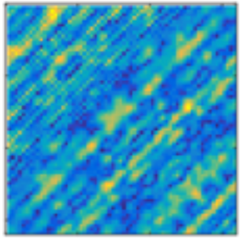

reflection matrix: **K**

Projection onto the single scattering basis

$$K_f = \sum_{m=1}^{2N-1} \langle K|E_m \rangle E_m$$

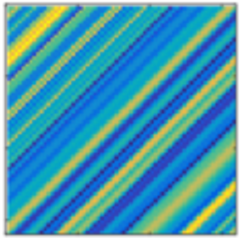

filtered matrix: $\mathbf{K_f}$

A. Baelde et al., Ultrasonics **82**, 379 (2018).

Theoretical single scattering space

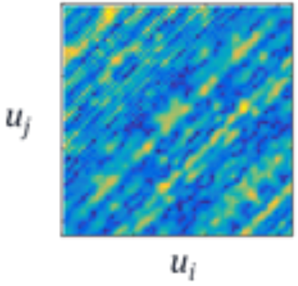

reflection matrix: **K**

Projection onto the single scattering basis

$$K_f = \sum_{m=1}^{2N-1} \langle K|E_m\rangle E_m$$

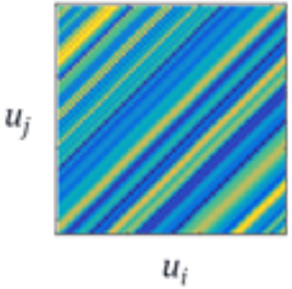

filtered matrix: $\mathbf{K_f}$

Single scattering weight estimator in the canonical basis:

$$\hat{\rho} = \frac{\|K_f\|^2}{\|K\|^2} \in [0;1]$$

$$\begin{cases} \hat{\rho} = 1 : & K \text{ only contains single scattering} \\ \hat{\rho} \to 0 : & K \text{ only contains multiple scattering} \end{cases}$$

A. Baelde et al., Ultrasonics **82**, 379 (2018).

Experimental single scattering estimators in titanium alloys

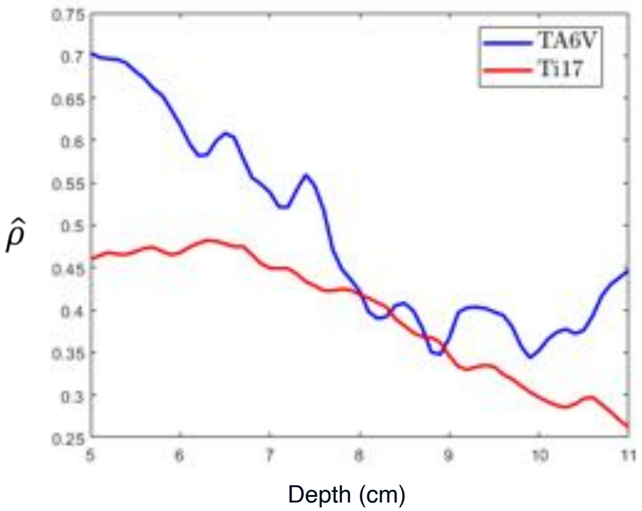

$$\hat{\rho} = \frac{\|K_f\|^2}{\|K\|^2} \in [0;1]$$

Frequencies: 2.8-3.2 MHz
Temporal windows: 5 μs
N = 128 transducers

Titanium alloys appear to be strong scatterers for the ultrasonic waves in the inspection frequency range.

Single scattering weight

- Is the estimator describing single scattering weight as expected?
- What is its bias?
- How is it linked to the physical parameters describing the medium (scattering mean-free path)?

Born series and scattering orders

Random distribution of scatterers with a speed contrast:

$$\mu(\boldsymbol{r}) = 1 - c_0^2/c(\boldsymbol{r})^2$$

Green's functions formalism:

$$G(\boldsymbol{r},\boldsymbol{r}',\omega) = G_0(\boldsymbol{r},\boldsymbol{r}',\omega)$$

$$+ k_0{}^2 \int G_0(\boldsymbol{r},\boldsymbol{r_1},\omega)\mu(\boldsymbol{r_1})G_0(\boldsymbol{r_1},\boldsymbol{r}',\omega)\, d\boldsymbol{r_1}$$

$$+ k_0^4 \iint G_0(\boldsymbol{r},\boldsymbol{r_1},\omega)\mu(\boldsymbol{r_1})G_0(\boldsymbol{r_1},\boldsymbol{r_2},\omega)\mu(\boldsymbol{r_2})G_0(\boldsymbol{r_2},\boldsymbol{r}',\omega)\, d\boldsymbol{r_1}\, d\boldsymbol{r_2}$$

$$+ \ \ldots$$

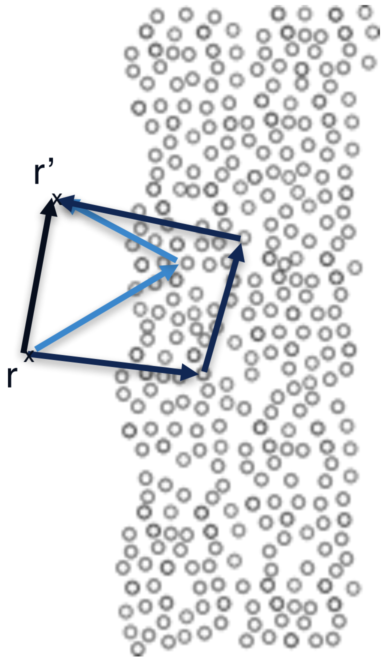

G	Green's function in a heterogeneous medium
G_0	Green's function in a homogeneous medium
μ	heterogeneity potential
k_0	wave vector

Single scatterer frequency response

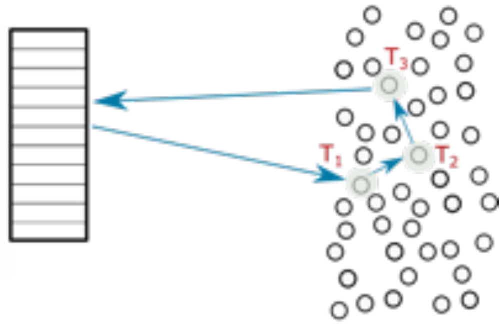

$$G_0(\boldsymbol{r},\boldsymbol{r}',\omega) = \begin{cases} -\frac{i}{4} H_0^{(1)}(k_0|\boldsymbol{r}-\boldsymbol{r}'|) & \text{in scalar 2D} \\ -\frac{\exp(ik_0|\boldsymbol{r}-\boldsymbol{r}'|)}{4\pi|\boldsymbol{r}-\boldsymbol{r}'|} & \text{in scalar 3D} \end{cases}$$

V scatterer volume
ρ_s scatterers density
σ_s scattering cross-section

- isotropic sub-wavelength fluid scatterers randomly distributed in the medium
- no attenuation
- longitudinal waves

- limited computation time compared to a more complex simulation

$$T_i\,(\boldsymbol{r_1},\boldsymbol{r_2},\omega) = T_0(\omega)\delta(\boldsymbol{r_1}\text{-}\boldsymbol{r_s})\,\delta(\boldsymbol{r_2}\text{-}\boldsymbol{r_s})$$

$$T_0(\omega) \approx \frac{k_0^2\mu(\boldsymbol{r_s})V}{1+\frac{ik_0^2\mu(\boldsymbol{r_s})V}{4}}$$ scatterer frequency response (2D)

- originality: separation of the reflection matrix into scattering orders
- allows to link the simulation to scattering parameters (independent scattering approximation, ISA):

$$l_s = \frac{1}{\rho_s\sigma_s} \qquad \sigma_s = \frac{|T_0(\omega)|^2}{4k_0}$$

Simulation of reflection matrices

$$K^{(1)}(\omega) = G_0(\omega)\times T_0(\omega)\times G_0^T(\omega)$$

$$K^{(n)}(\omega) = G_0(\omega)\times T_0(\omega)\times\left(G_0'(\omega)\times T_0(\omega)\right)^{n-1}\times G_0^T(\omega) \qquad \forall n > 1$$

$$K(\omega) = G_0(\omega)\times T_0(\omega)\times\left(I - G_0'(\omega)\times T_0(\omega)\right)^{-1}\times G_0^T(\omega)$$

Absolute value of the matrix elements at central frequency

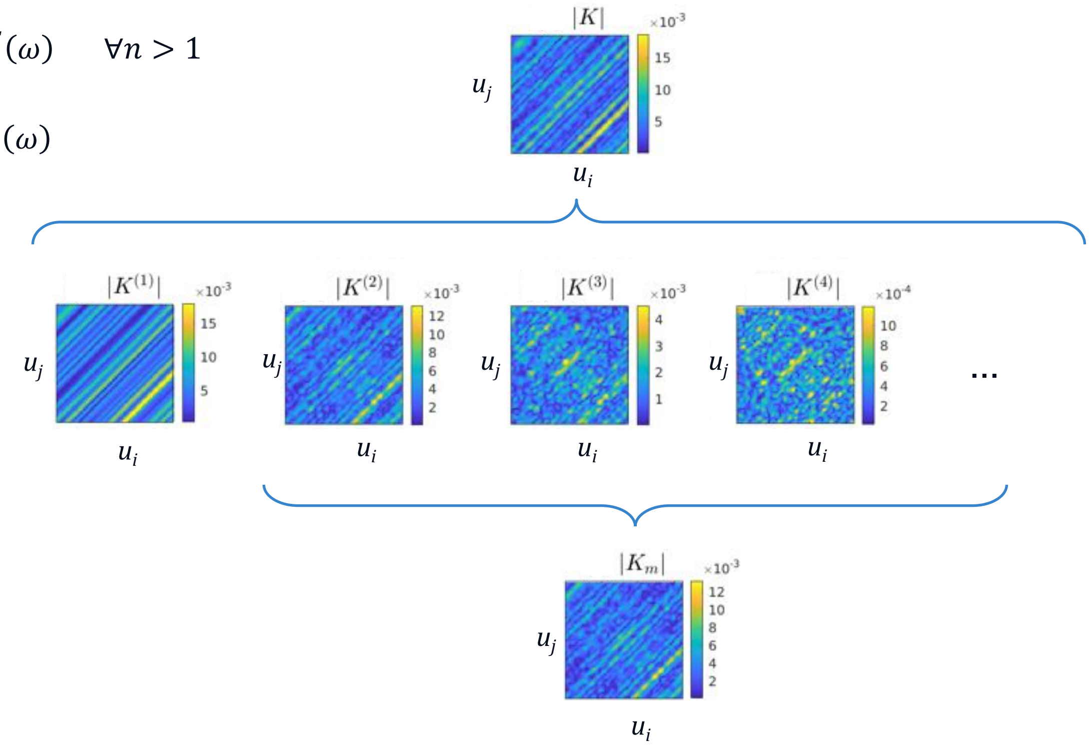

f	1-2 MHz
c_0	1480 m/s
c_s	2500 m/s
ρ_s	4 /cm²
z	14-27.5 cm

Reflection matrix properties

Impulse response properties

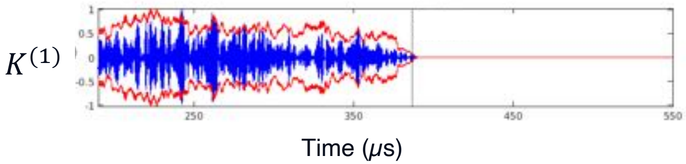

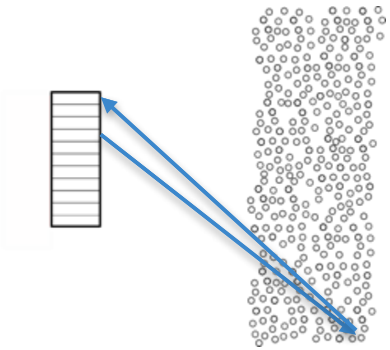

Reflection matrix properties

Impulse response properties

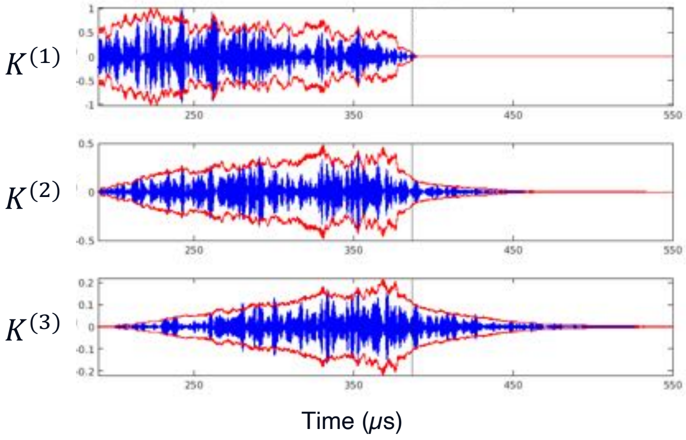

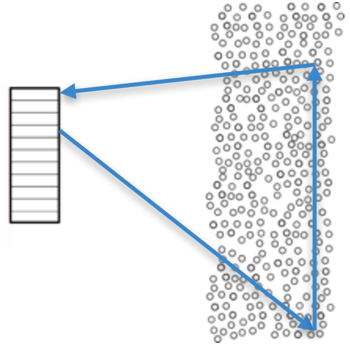

Reflection matrix properties

Impulse response properties

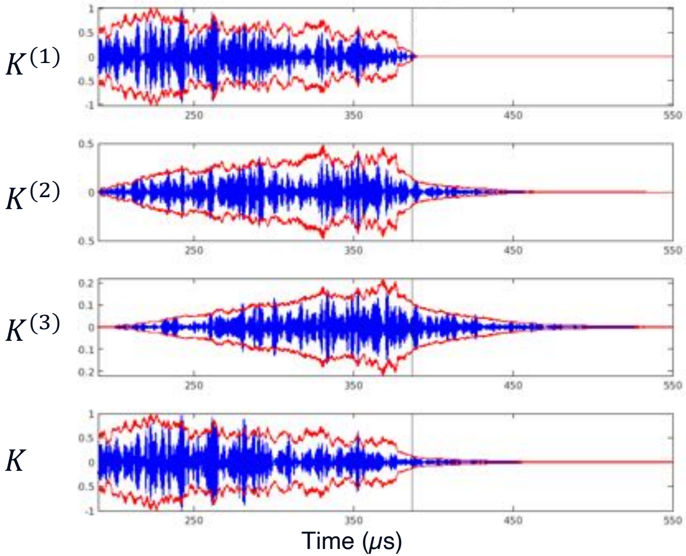

Mean backscattered intensity

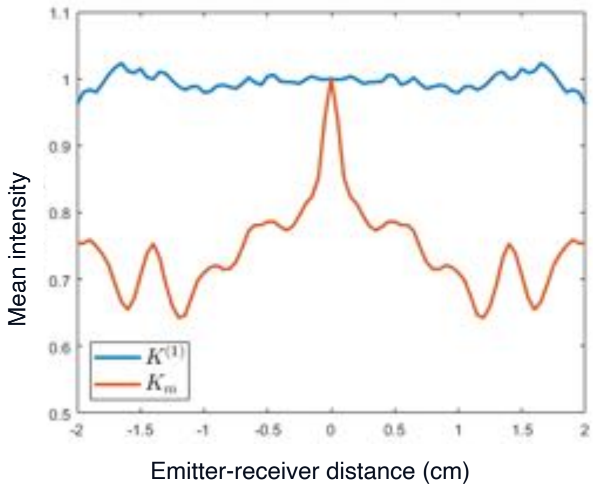

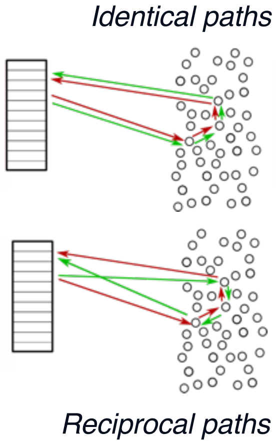

Coherent backscattering peak: signature of the presence of multiple scattering

A. Ishimaru et al., J. Opt. Soc. Am., JOSA **73**, 131 (1983).

Single scattering weight and its estimator

Single scattering weight estimator: $\hat{\rho} = \dfrac{\|\boldsymbol{K_f}\|^2}{\|\boldsymbol{K}\|^2} \in [0;1]$

Single scattering weight: $\rho = \dfrac{\|\boldsymbol{K}^{(1)}\|^2}{\|\boldsymbol{K}\|^2}$

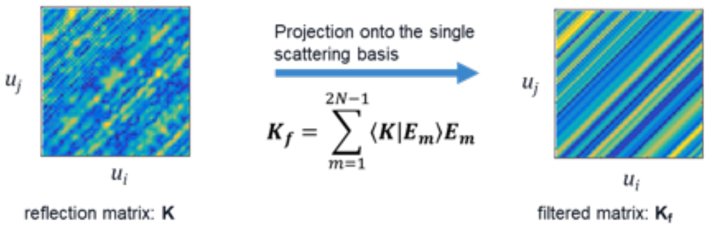

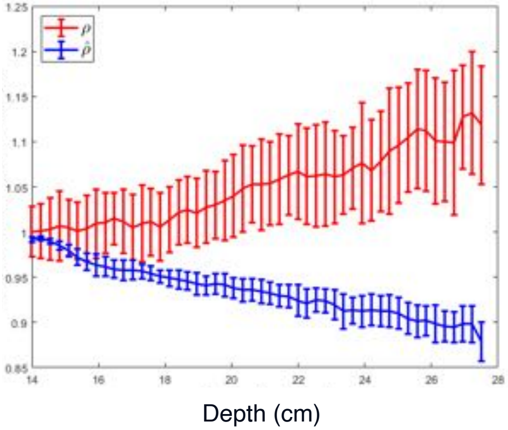

$$\|\boldsymbol{K}^{(1)}\|^2 > \|\boldsymbol{K}\|^2 = \|\boldsymbol{K}^{(1)} + \boldsymbol{K}^{(2)} + \cdots\|^2$$

thus, it exists some correlation between the scattering orders.

$$\Pi(\boldsymbol{K}^{(n)}) = \frac{|\langle \boldsymbol{K}^{(n)} | \boldsymbol{K}^{(1)} \rangle|}{\|\boldsymbol{K}^{(n)}\| \, \|\boldsymbol{K}^{(1)}\|}$$

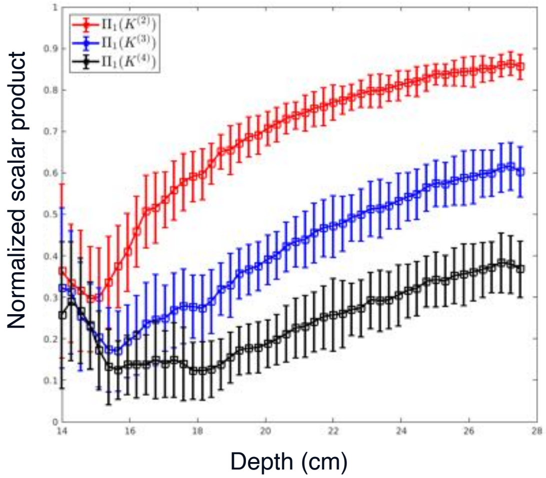

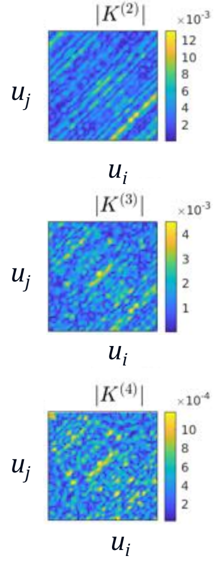

Recurrent scattering contribution

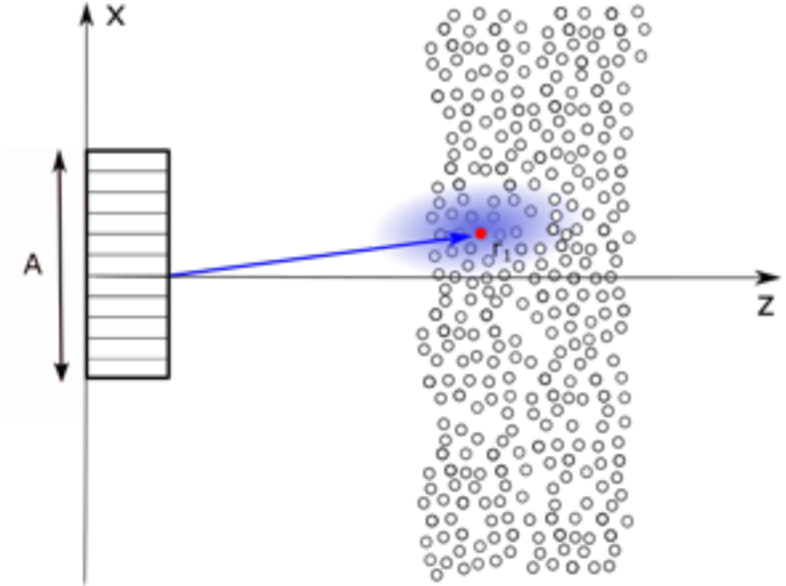

Probe resolution cell size:

$$\begin{cases} \delta_x = \dfrac{\lambda z}{A} \\ \delta_z = \dfrac{7\lambda z^2}{A^2} \end{cases}$$

Recurrent scattering contribution

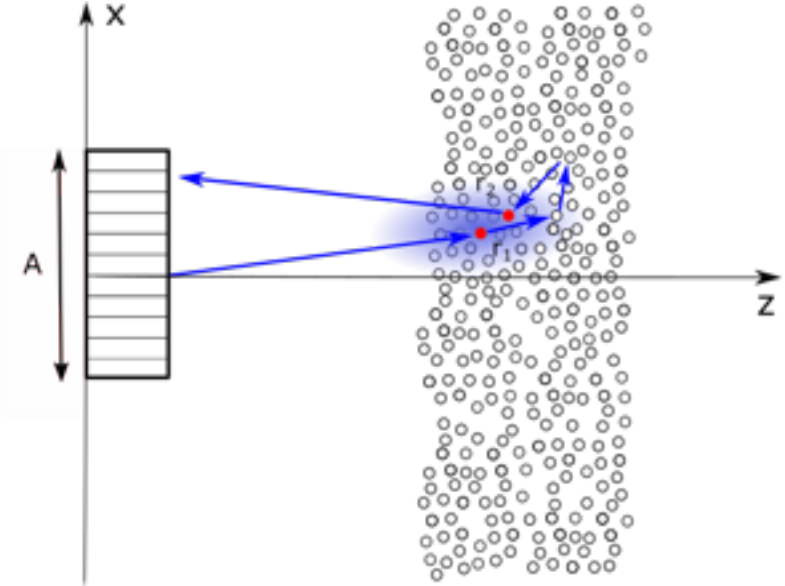

Probe resolution cell size:

$$\begin{cases} \delta_x = \dfrac{\lambda z}{A} \\ \delta_z = \dfrac{7\lambda z^2}{A^2} \end{cases}$$

Recurrent scattering: paths for which the first and last scatterers are located in the same resolution cell.

$|K_r|$

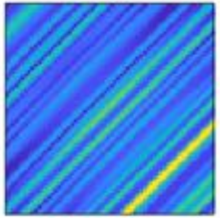

u_j

u_i

The filter does not allow to separate the single and the recurrent scattering contributions, which both display the memory effect.

A. Aubry et al., Phys. Rev. Lett. **112**, 043903 (2014).

Confocal scattering matrix

Separation into confocal scattering (single + recurrent) and conventional multiple scattering.

Absolute value of the matrix elements at central frequency

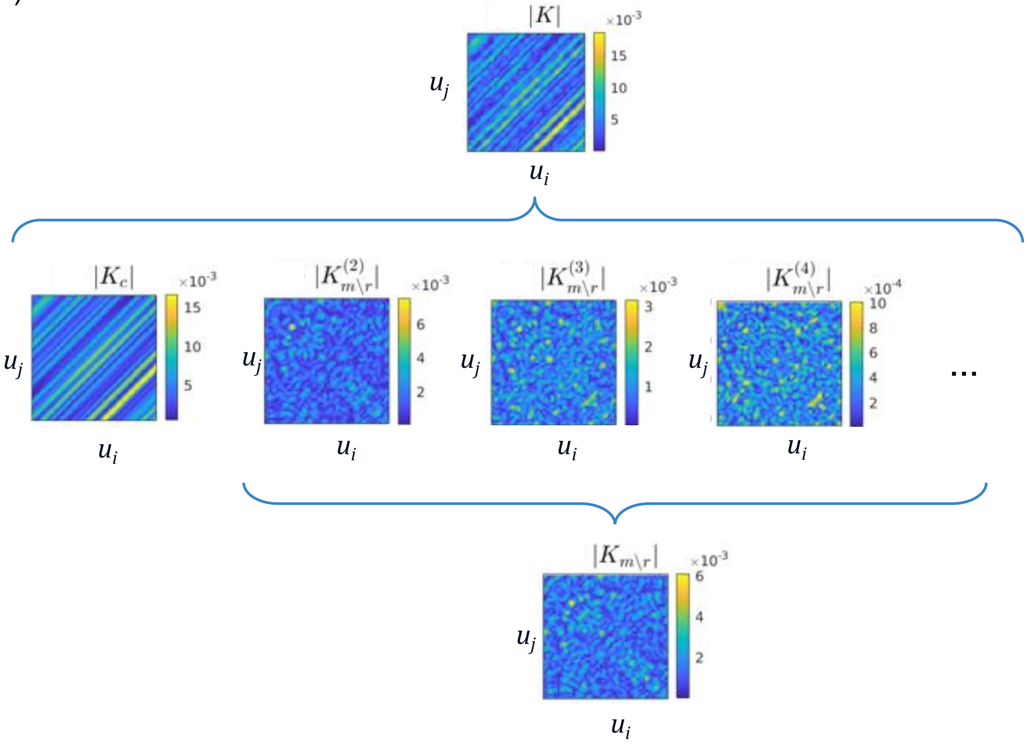

f 1-2 MHz
c_0 1480 m/s
c_s 2500 m/s
ρ_s 4 /cm²
z 14-27.5 cm

Single and confocal scattering weight

Single scattering weight estimator: $\hat{\rho} = \frac{\|\boldsymbol{K}_f\|^2}{\|\boldsymbol{K}\|^2} \in [0;1]$

Single scattering weight: $\rho = \frac{\|\boldsymbol{K}^{(1)}\|^2}{\|\boldsymbol{K}\|^2}$

Confocal scattering weight: $\rho_c = \frac{\|\boldsymbol{K}_c\|^2}{\|\boldsymbol{K}\|^2}$

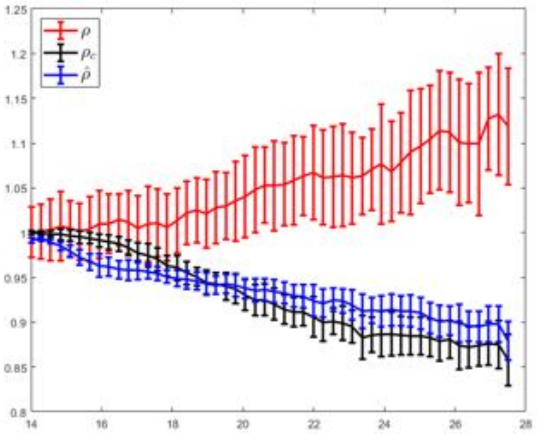

Depth (cm)

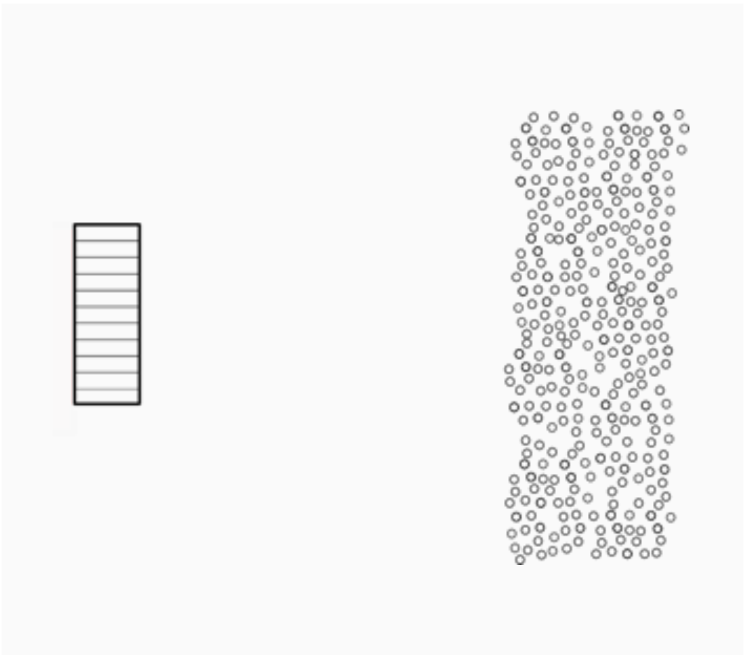

The estimator deals with the confocal scattering weight and not the single scattering weight.

Single and confocal scattering weight

Single scattering weight estimator: $\hat{\rho} = \frac{\|\boldsymbol{K}_f\|^2}{\|\boldsymbol{K}\|^2} \in [0;1]$

Single scattering weight: $\rho = \frac{\|\boldsymbol{K}^{(1)}\|^2}{\|\boldsymbol{K}\|^2}$

Confocal scattering weight: $\rho_c = \frac{\|\boldsymbol{K}_c\|^2}{\|\boldsymbol{K}\|^2}$

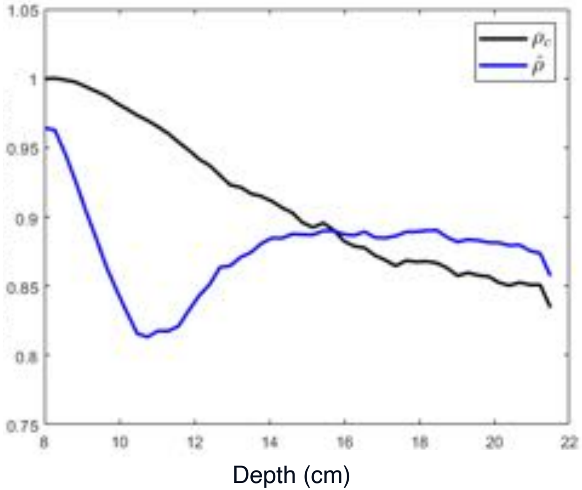

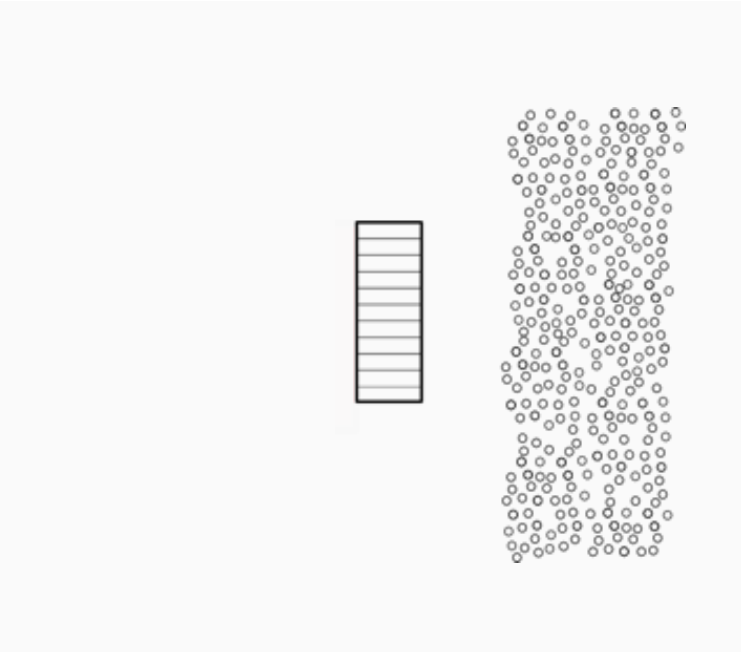

When the paraxial approximation is not valid, the estimator is not exact.

Estimators in the focused basis

$K(u_i, u_j, t)$ $\qquad\qquad$ $\bar{R}(x_{in}, x_{out}, z)$

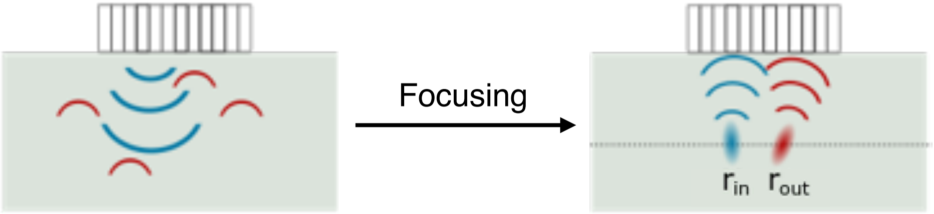

- contributions close to the main diagonal: mainly linked to single scattering ;
- contributions far from the main diagonal: linked to multiple scattering.

$\overline{R^{(1)}}$

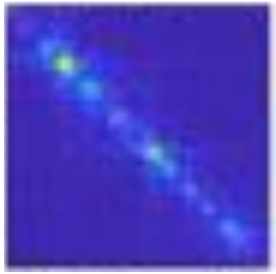

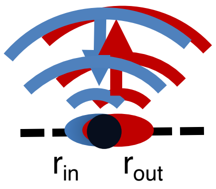

$\overline{R_{m\backslash r}}$

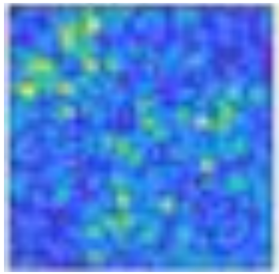

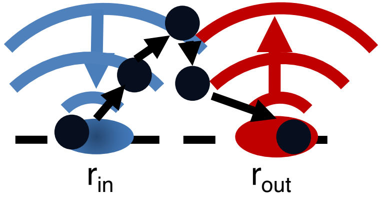

Estimators in the focused basis

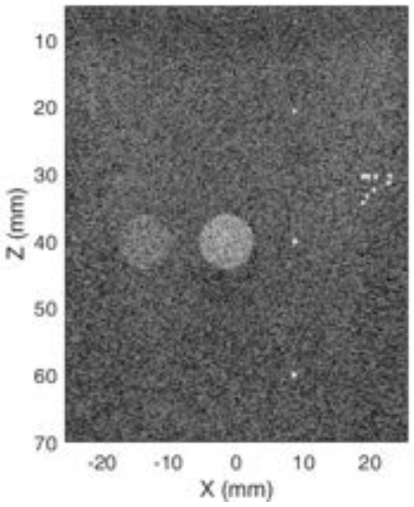

Echographic image
Contrast: impedence mismatch

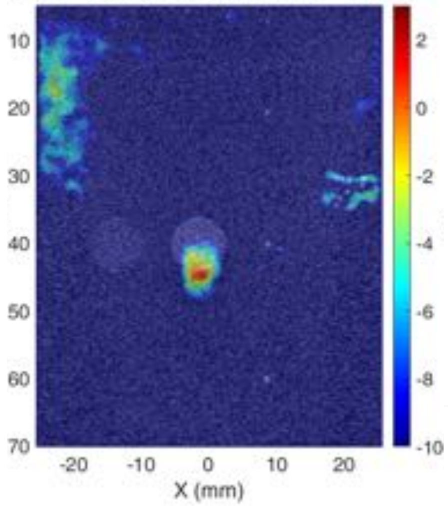

Contrast: multiple scattering weight

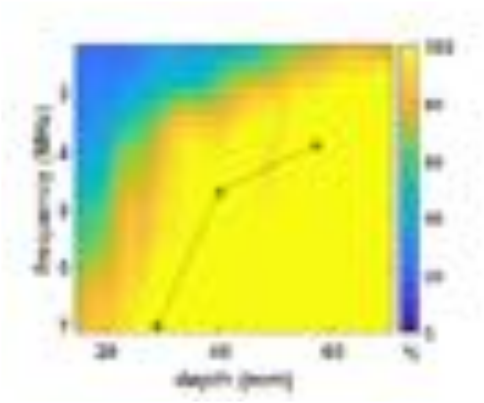

Multiple scattering proportion in a copper sample

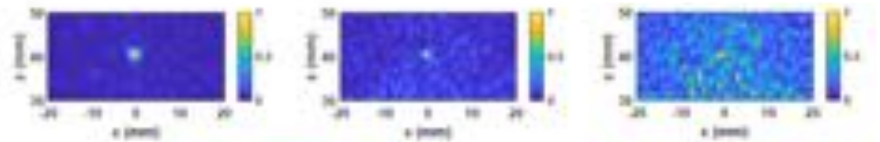

Flaw at depth 4 cm imaged at 2.5, 3.5 et 4.7 MHz.

W. Lambert, PhD manuscript (2020). A. Velichko, IEEE Trans. Ultrason., Ferroelect., Freq. Contr. **67**, 92 (2020).

Confocal scattering weight in the focused basis

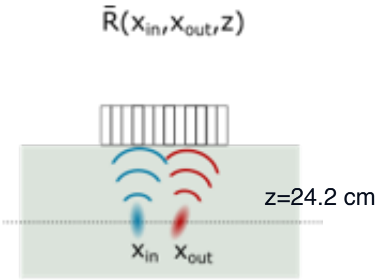

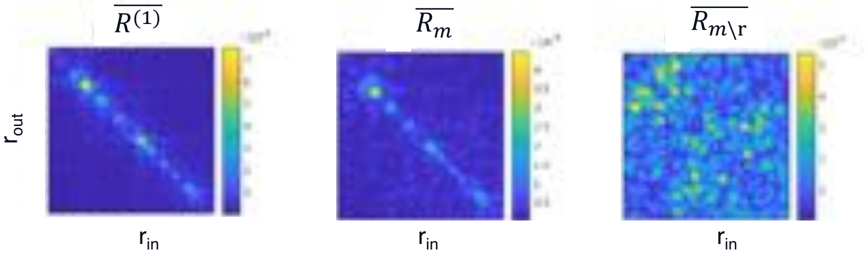

How to build a theoretical confocal scattering space in the focused basis?

f	1-2 MHz
c_0	1480 m/s
c_s	2500 m/s
ρ_s	4 /cm²
z	14-27,5 cm

Confocal scattering space in the focused basis

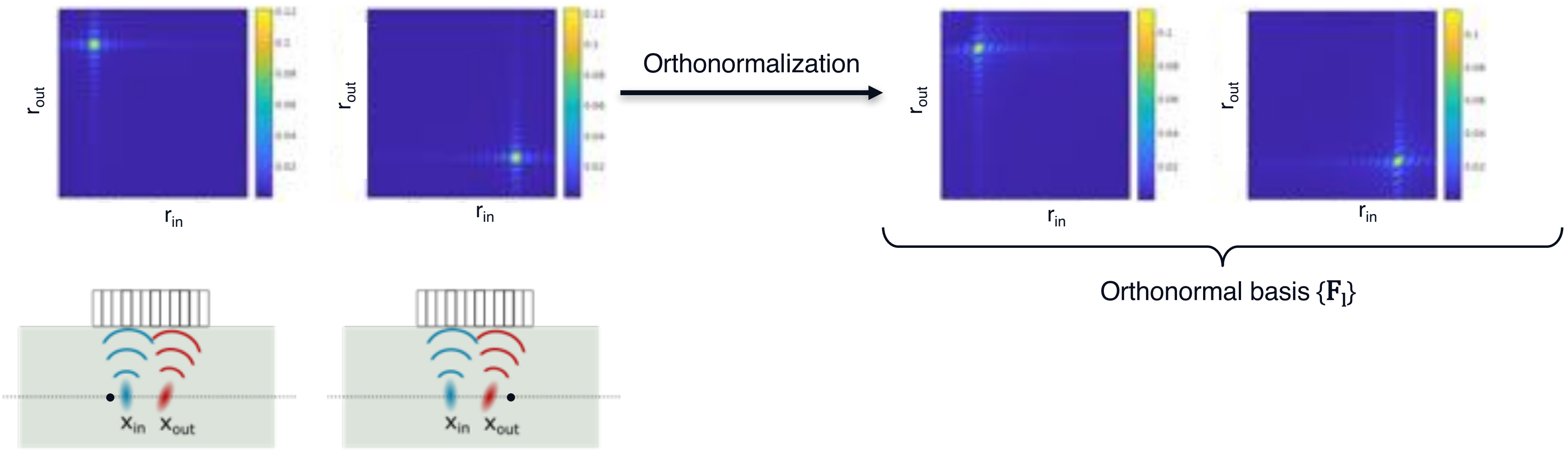

Filtering of the total scattering matrix:

$$\boldsymbol{R_f} = \sum_{l} \langle \boldsymbol{F_l} | \boldsymbol{R} \rangle \boldsymbol{F_l}$$

Confocal scattering weight estimator:

$$\hat{\rho}_f = \frac{\|\overline{\boldsymbol{R}}_f\|^2}{\overline{\|\overline{\boldsymbol{R}}\|^2}}$$

Single and confocal scattering weights in the focused basis

Confocal scattering weight estimator:

$$\hat{\rho}_f = \frac{\|\overline{\boldsymbol{R}_f}\|^2}{\|\overline{\boldsymbol{R}}\|^2}$$

« True values » obtained by simulation:

$$\rho_f = \frac{\|\overline{\boldsymbol{R}^{(1)}}\|^2}{\|\overline{\boldsymbol{R}}\|^2}$$

$$\rho_{fc} = \frac{\|\overline{\boldsymbol{R}_c}\|^2}{\|\overline{\boldsymbol{R}}\|^2}$$

f	1-2 MHz
c_0	1480 m/s
c_s	2500 m/s
ρ_s	4 /cm²
z	14-27.5 cm

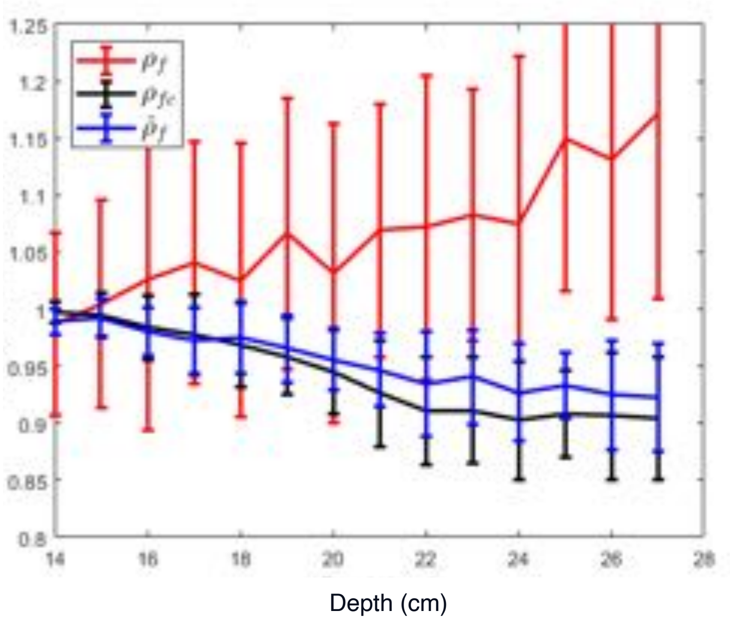

Focused basis advantages

The paraxial approximation is not required in the focused basis.

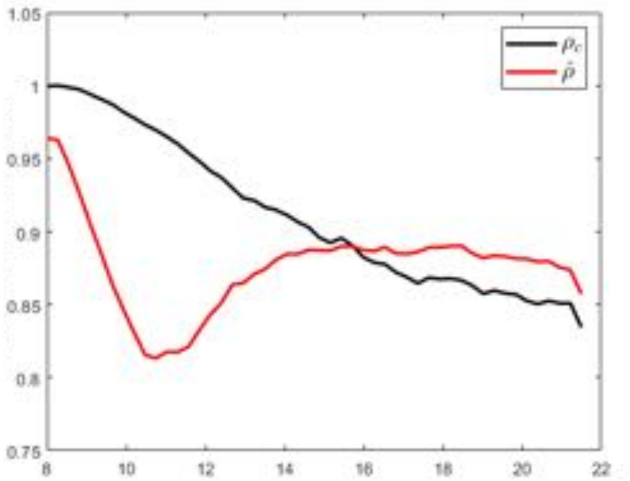

Depth (cm)

Focused basis advantages

The paraxial approximation is not required in the focused basis.

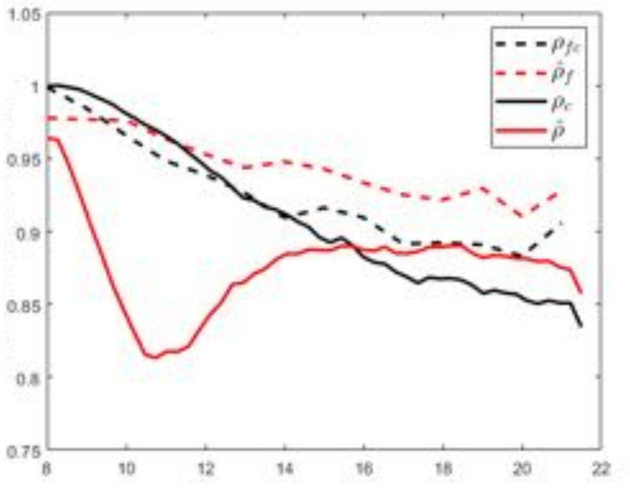

Natural basis to image the medium:

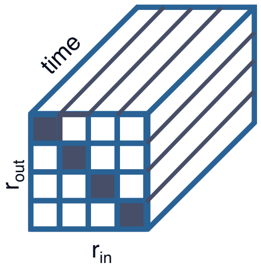

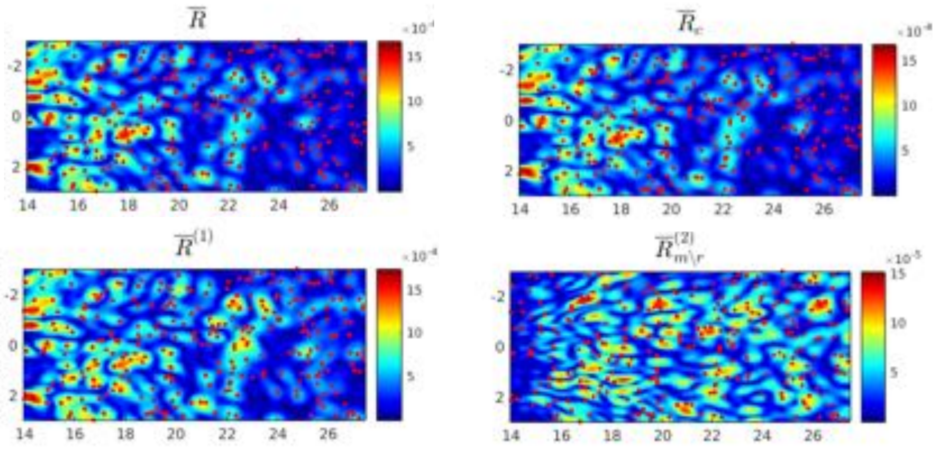

Link with the scattering mean-free path

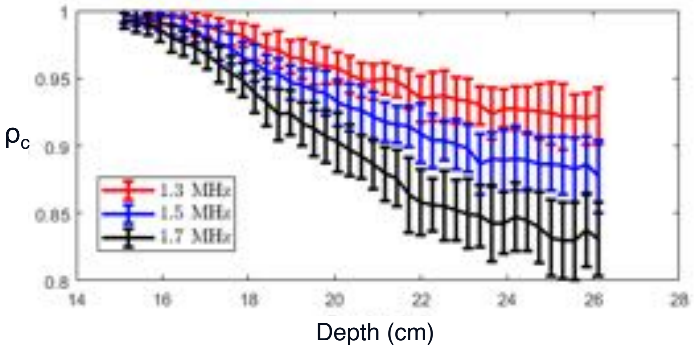

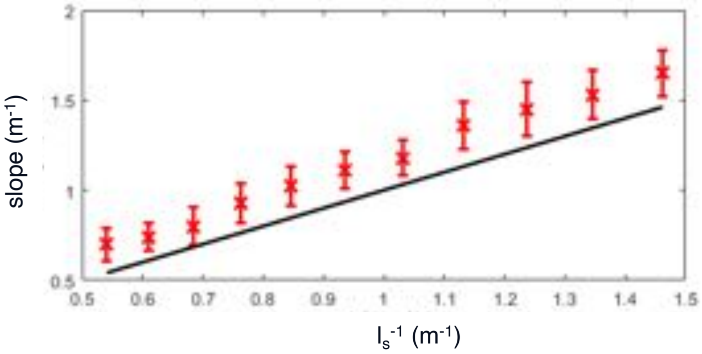

$$l_s = \frac{1}{\rho_s \sigma_s} \qquad \sigma_s = \frac{|T_0(\omega)|^2}{4k_0}$$

The slope of the confocal scattering weight estimator seems correlated with the scattering mean-free path.

Conclusion and perspectives

- The estimators built in the literature are estimators of confocal scattering rather than single scattering.
- Single and recurrent scattering have very similar properties: it is complex to separate them.
- Recurrent scattering triggers correlations between the scattering orders: $I \neq I_1 + I_m$.
- The focused basis allows to locally estimate the confocal scattering weight, without any assumption.

$$\Pi\left(\mathbf{K}^{(n)}\right) = \frac{\left|\langle \mathbf{K}^{(n)} | \mathbf{K}^{(1)} \rangle\right|}{\left\|\mathbf{K}^{(n)}\right\| \left\|\mathbf{K}^{(1)}\right\|}.$$

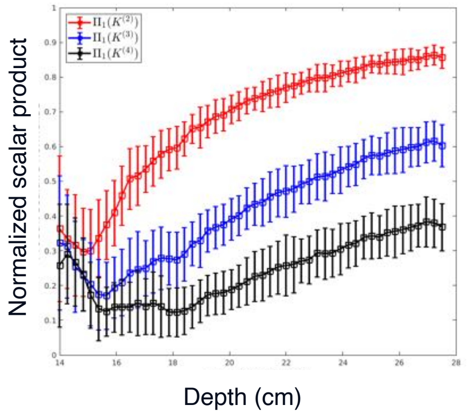

C. Brütt et al., Phys. Rev. E **106**, 025001.